THE MEASUREMENT OF TWISS PARAMETERS USING SEGMENTED FARADAY CUPS*

M. Rosing, C. Hummer, R. Zolecki
Argonne National Laboratory
9700 S. Cass Avenue, EP/207
Argonne, IL 60439

Introduction

The Segmented Faraday Cup (SFC) consists of 48 copper plates that are 1 mm × 75 mm × 10 mm. these plates are stacked against each other on the 75 mm × 10 mm face with a layer of kapton between them for electrical insulation. When the assembly is viewed in the direction of the incident beam, the beam sees 48 vertical electrodes that are 1 mm × 75 mm and 10 mm thick. The copper plates and the kapton are held together in an aluminum frame which is mounted on a rotating shaft.

The charge collected by each electrode is stored on a capacitor. The voltage on each of these capacitors is sequentially presented to a buffer amplifier, and the profile of the beam can then be read out. timing pulses are provided during the readout to trigger the analog to digital converter (ADC). Each time the ADC receives one of these timing pulses, it digitizes the voltage from the buffer amplifier. A computer then stores these data for documentation and further study, or the computer may use the data for on-line calculations.

The SFCs were used to measure the emittance of the beam by using a scanning slit. The theory and the method for this measurement are presented in Section I. A description of the electronics is presented in Section II. A sample of a beam profile and the results of an emittance measurement are presented in Section III.

I. Measurements of Beam Distributions

The actual beam distribution is a function of four variables, $D(X, Y, \theta_x, \theta_y)$, when it is assumed that the beam has no momentum spread. X and Y are the horizontal and vertical spatial coordinates of a particle as it passes through the plane of the slit. θ_x and θ_y are the angles between the path of the particle and the X-axis and the Y-axis respectively. Since θ_x is proportional to the X component of the momentum and θ_y is proportional to the Y component of the momentum, the actual beam distribution may be interpreted to be a function of the position of the particle and the momentum of the particle, or the beam has some distribution in the four-dimensional phase space of space and momentum. If the beam had a momentum spread, then the actual beam distribution would be a function of six variables, and it would have a distribution in the six-dimensional phase space.

The four-dimensional phase space distribution $D(X, Y, \theta_x, \theta_y)$ is not measured by the scanning slit and the SFC, rather is it an integral over a spatial coordinate and angle. When the slit is oriented with edges parallel to the y-axis, as shown in Figure 1, the fact that a particle will pass through the slit or not depends only on the X coordinate. The total

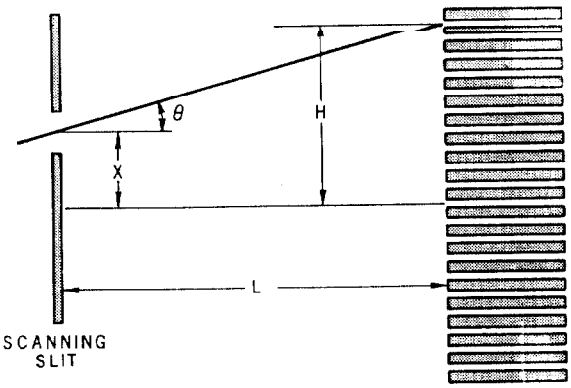

Figure 1: Angular distribution measured by SFC

number of particles passing through the slit is then the integral of the four-dimensional beam distribution over all values of Y. Once a particle passes through the slit, the particle will strike a segment of the SFC, if it has a given angle θ_x, since it is fixed by $\theta_x = (H - X)/L$. H is the distance of the segment from the center line, X is the distance of the slit from the center line, and L is the distance from the slit to the SFC as shown in Figure 1. This segment will collect all particles with this given angle θ_x and for all angles θ_y (Figure 1). Thus the total current collected by a given segment for a given position of the slit is the integral of the actual beam distribution over all values of Y and θ_y. By stepping the slit across the beam and recording the angular distribution at each step, the beam distribution as a function of X and θ_x is measured. And, if the slit and the SFC are rotated by 90 degrees, the beam distribution as a function of y and θ_y can be measured. These measured beam distributions could be determined from the actual four-dimensional phase space distribution by integrating over Y and θ_y for the X and θ_x distribution, or by integrating over X and θ_x for the Y and θ_y distribution. Thus

$$F(X,\theta_x) = \int_{-\pi}^{\pi} d\theta_y \int_{-\infty}^{\infty} D(X,Y,\theta_x,\theta_y)dY$$

$$G(Y,\theta_y) = \int_{-\pi}^{\pi} d\theta_x \int_{-\infty}^{\infty} D(X,Y,\theta_x,\theta_y)dX \qquad (1)$$

The four-dimensional phase space distribution, however, cannot be determined from the two two-dimensional phase space distributions, $F(X,\theta_x)$ and $G(Y,\theta_y)$, alone. Still, these two two-dimensional phase space distributions do provide valuable information.

The measurement of $F(X,\theta_x)$ requires that the angular distributions be recorded as the slit is being

*This work was performed under the auspices of the U.S. Department of Energy under Contract W-31-109-ENG-38 and was supported by the U.S. Army Strategic Defense Command.

CH2669-0/89/0000-1586$01.00©1989 IEEE

scanned across the beam from one side of the beam to the other side of the beam. This procedure is automated by a MicroVAX 780 computer. The computer records the angular distribution and then moves the slits to a new location for another angular distribution. When the angular distributions are plotted in Figure 2 for each position of the slit, it seems that the distribution is a two-dimensional Gaussian distribution. Thus, it is assumed that the distribution of the beam is

$$J(X,\theta_x) = J_0 \mathrm{Exp}\left(\frac{-\gamma X^2 + 2\alpha X\theta_x - \beta\theta_x^2}{\varepsilon_0}\right) \qquad (2)$$

where α, β and γ are the Twiss parameters, and ε is the emittance of the beam. Since α, β, and γ must satisfy the relation $\gamma\beta-\alpha^2 = 1$, there are four free parameters for fitting the data, α, β, ε, and J_0. J_0 in this instance is considered to be an arbitrary scaling factor, since the data were rescaled.

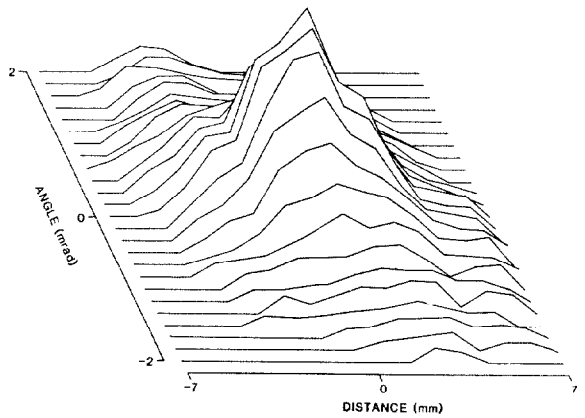

Figure 2: Measured emittance (angular distribution as a function of slit position).

The data shown in Figure 2 were fitted to this functional form by using the Lenard-Marquart method [2]. In this case, each datum point was weighted by the expected error which were,

$$\sigma^2(X,\theta_x) = \frac{J^2(X,\theta_x)}{100} + 9 \qquad (3)$$

One source of error is the variation of the storage capacitors. If each of these capacitors was given an equal amount of charge, the voltage across these capacitors would vary by ten percent. Since the buffer amplifier is a voltage amplifier, the variation in the capacitance is a source of error. A charge-sensitive amplifier will be used in the next modification to eliminate this source of error. The next source of error is noise. In the regions where no beam current was collected by an element, the data had background counts with a standard deviation of about 3.0. Adding these two sources of error in quadrature gives the weighting function (3). The results of the fitting to the weighted function are

α = 0.33 ± 0.02
β = 4.03 ± 0.03
γ = 0.275 ± 0.002
ε_0 = 4.09 πmm rad
χ^2 = 1.54

for the data shown in Figure 5. χ^2 has been divided by the number of datum points plus the number of fitting parameters minus 2. The errors on the fitting parameters were estimated by a Monte-Carlo calculation. A pseudo-random number with a Gaussian distribution and having a standard deviation of the weighting function was added to the original data. These new data were refitted giving a new set of fitted parameters which were recorded. The errors of the above parameters are the standard deviation of the fitted parameters for a number of fittings.

II. Description of the SFC Electronics

The details of the electronics for the SFC were previously described [1], but a summary of the electronics is presented here. There are three analog switches for each element of the SFC as shown in Figure 3. Each switch can be opened or closed by a digital control signal. The first switch, SW1, grounds the element to prevent it from collecting a charge before the sampling time. The second switch, SW2, is part of a sample and hold circuit. SW2 is also closed at the start of the sampling time. Sampling begins by opening SW1. The beam current that is collected by the element is now charging the capacitor for the duration of the sampling time. At the end of the sampling time, SW2 is opened to prevent the charged capacitor from discharging to ground. SW1 is closed to ground the element after SW2 is opened. The charge collected by the element during the sampling time is now stored in the capacitor. The capacitor can then be connected to an amplifier via a bus line by closing SW3. This permits the multiplexing of each of the segment storage capacitors to the amplifier. The output of the amplifier is then a serial output of the voltage on each of the capacitors multiplexed in time.

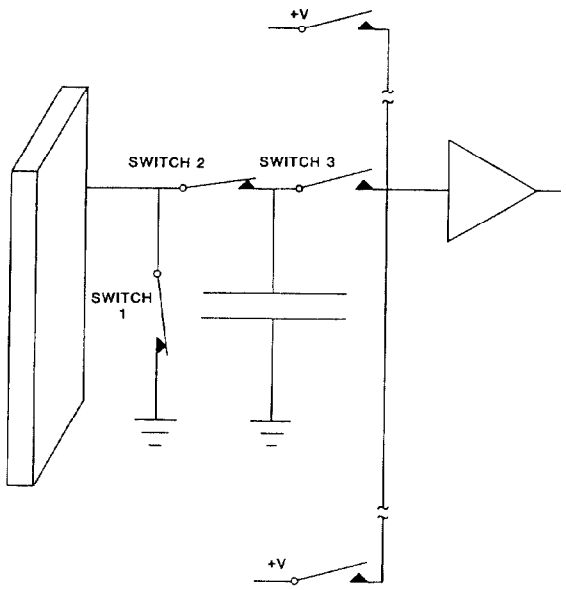

Figure 3: SFC electronics.

A timing mark at the start of the output scan is generated by having the first multiplexing switch connected to a voltage source rather than to a capacitor. When this multiplexing switch is opened at the start of the readout, a constant voltage is placed on the common input of the output amplifier. This voltage, which is larger than the voltage that is

usually collected by the capacitor, signals the start of the output scan. This signal may be used to trigger an oscilloscope to display the output signal. Another timing mark is generated at the end of the scan by another multiplexing switch that is connected to a voltage source. This voltage mark at the end of the scan is used to set the horizontal scale on the oscilloscope. Once the horizontal scale of the oscilloscope is set, the oscilloscope displays the profile of the beam on a scale where the center of the horizontal trace corresponds to the center of the beam line. Thus the oscilloscope gives a graphical display of the position and the shape of the beam.

To enhance the signal-to-noise ratio, the SFC electronics were gated twice, once with beam on and 100 milliseconds later with beam off. The analog-to-digital conversion was performed by a local 8-bit microprocessor, and both sets of data were stored. The beam-off data were subtracted from the beam-on data to remove systematic differences in storage capacitors, cable lengths, and other problems. These values were then sent through a digital-to-analog converter at the same clock speed as the incoming data. In this way, very clean signals were observed even at low beams of 100 microamps.

III. Results

Figure 4a shows a typical oscilloscope trace. The initial and final element markers are set so that 'scope center corresponds to the physical center of the beam line. Using a storage oscilloscope, it is very easy to monitor changes of magnets and beam profile on a pulse-to-pulse basis.

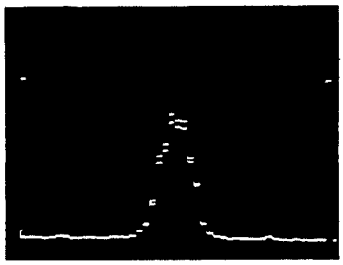

a

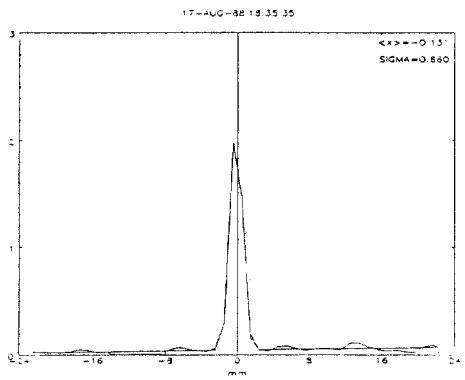

b

Figure 4: a) Raw and b) Digitized output.

Figure 4b shows a typical computer trace. The markers have been removed, and the profile is drawn as connected lines. Once profile data are stored on disk, it is very easy to find centroid and width information (shown in the top right). While useful, the computer is too slow to give this data in real time. Thus, we find that the oscilloscope trace can get very quick results, then we wait for the computer analysis to "fine tune" better than the eye. The result is a beam which is centered in the beam line to within .2 mm, even though we have only 1 mm resolution.

Figure 5 shows processed emittance data. Each SFC profile has been compared so that only percentage amplitude information is presented. These data were taken just after the linac and represent the initial vertical emittance. By fitting Twiss parameters to this data, one can then use TRANSPORT or similar codes to initially set magnets for beam tuning. Various programs have been written to manipulate this data

	-6	-5	-4	-3	-2	-1	0	1	2	3	4	5	6	7	SUM 8ROW
2.07			7	13	11	4									6
1.98			11	11	13	9									7
1.90			5	14	13	8	5	4							8
1.81		4	9	10	16	6	8	5	4						11
1.73		4	15	14	11	9	8	7	4	4					13
1.65		4	12	17	13	6	7	4	7	5					13
1.56			11	16	16	9	5	8	6	5					13
1.48			15	16	17	14	10	8	8	7		6			18
1.39			11	19	18	13	13	7	5	6		6			17
1.31		4	14	17	19	13	12	14	9	5	5	7			21
1.22		5	11	19	17	16	15	14	17	9		7			23
1.14		6	18	17	22	15	17	16	15	13	5				25
1.06		9	16	22	18	18	18	20	18	13	10	7			30
0.97		9	18	25	24	17	27	20	26	18	12	11			37
0.89		7	20	26	25	27	28	30	22	23	13	11	5		42
0.80		5	21	27	29	31	40	32	34	23	17	12	4		49
0.72	4	11	17	27	31	35	45	47	34	31	16	13	4		56
0.63		9	23	28	35	38	53	48	49	33	22	10	9	4	65
0.55		9	19	32	31	45	63	61	51	40	20	13	7		70
0.46		5	22	30	40	49	71	69	61	40	29	11	9		78
0.38		11	18	32	35	63	73	74	64	48	29	14	7	4	85
0.30		6	21	27	44	60	94	74	67	49	33	15	11		90
0.21		7	18	34	36	73	82	100	65	50	31	15	10	5	94
0.13			17	32	47	64	99	80	87	48	36	15	14	10	99
0.04		4	15	33	38	75	84	95	67	59	31	16	13	11	97
-0.04		7	15	27	45	66	94	80	82	50	41	11	15	8	97
-0.13			13	25	33	62	85	89	61	55	33	15	12	11	89
-0.21		5	12	25	34	50	82	76	67	44	37	17	19	9	86
-0.30			11	18	31	55	64	72	53	46	28	16	14	11	75
-0.38			9	15	27	36	64	57	56	40	33	12	16	9	67
-0.46			7	16	20	42	51	55	44	38	28	17	13	12	4 62
-0.55				13	20	25	49	44	44	32	29	13	16	9	53
-0.63			4	8	16	30	34	41	37	34	25	14	13	15	48
-0.72			4	11	12	25	33	31	33	29	25	9	14	12	5 43
-0.80			7	9	11	17	24	32	25	28	23	12	11	10	4 38
-0.89				6	11	17	16	23	27	24	25	13	12	9	33
-0.97				8	10	16	16	17	22	23	16	7	12	13	28
-1.06				4	11	11	12	16	15	22	21	9	11	10	25
-1.14				6	6	8	9	14	17	16	16	11	11	7	21
-1.22				5	8	5	10	11	14	15	15	6	9	11	19
-1.31					9	5	9	14	13	17	16	4	12	10	19
-1.39				5	5	4	9	9	14	12	13	4	6	8	16
-1.48				5	4	5	7	8	10	13	10	7	8		13
-1.56					5		4	9	8	11	14	5	6	5	12
-1.65							5	6	10	10	11	6	7	5	10
-1.73							4	8	5	9	9		5		7
-1.81								4	6	8	9		4	4	6
-1.90									5	7	7	4		4	4
-1.98										7	5				2
SUM COL =	0	8	29	48	59	75	99	98	88	71	50	25	21	14	0

Figure 5: Processed emittance data.

depending on what desired emittance was required at the end of the beam line. the vertical dimension is milliradians, and the horizontal is millimeters.

IV. Summary

While SFC technology is relatively old, the ability to combine the data using computers allows much more flexibility than just being able to center the beam in the pipe. Emittance measurements in two dimensions are straightforward and automatic. Beam center and width can be matched to expected values from beam optics codes, and magnets can be adjusted for corrections to very fine resolution. In the future, we hope that higher-speed computers will allow this information to be gathered and presented in real time so that operators can tune the line very quickly and easily.

References

[1] R. L. Kustom, et al., IEEE Trans. Nucl. Sci., vol. 20, no. 3, pp. 518-522, 1973.

[2] W. H. Press, B. P. Flannery, S. A. Teukolsky, W. T. Vetterling, Numerical Recipes, Cambridge University Press, 1986, ch. 14.